



## Low-lying proton intruder state in $^{13}\text{B}$

S. Ota<sup>a,\*</sup>, S. Shimoura<sup>a</sup>, H. Iwasaki<sup>b</sup>, M. Kurokawa<sup>c</sup>, S. Michimasa<sup>a</sup>, N. Aoi<sup>c</sup>, H. Baba<sup>c</sup>, K. Demichi<sup>d</sup>, Z. Elekes<sup>e</sup>, T. Fukuchi<sup>c</sup>, T. Gomi<sup>c</sup>, S. Kanno<sup>c</sup>, S. Kubono<sup>a</sup>, K. Kurita<sup>d</sup>, H. Hasegawa<sup>d</sup>, E. Ideguchi<sup>a</sup>, N. Iwasa<sup>f</sup>, Y.U. Matsuyama<sup>d</sup>, K.L. Yurkewicz<sup>g</sup>, T. Minemura<sup>c</sup>, T. Motobayashi<sup>c</sup>, T. Murakami<sup>h</sup>, M. Notani<sup>i</sup>, A. Odahara<sup>j</sup>, A. Saito<sup>b</sup>, H. Sakurai<sup>c</sup>, E. Takeshita<sup>c</sup>, S. Takeuchi<sup>c</sup>, M. Tamaki<sup>a</sup>, T. Teranishi<sup>k</sup>, Y. Yanagisawa<sup>c</sup>, K. Yamada<sup>c</sup>, M. Ishihara<sup>c</sup>

<sup>a</sup> Center for Nuclear Study, University of Tokyo, Saitama 351-0198, Japan

<sup>b</sup> Department of Physics, University of Tokyo, Tokyo 113-0033, Japan

<sup>c</sup> RIKEN Nishina Center for Accelerator-Based Science, Saitama 351-0198, Japan

<sup>d</sup> Department of Physics, Rikkyo University, Tokyo 171-8501, Japan

<sup>e</sup> Hungarian Academy of Sciences, Institute of Nuclear Research, H-4001 Debrecen, Hungary

<sup>f</sup> Department of Physics, Tohoku University, Miyagi 980-8578, Japan

<sup>g</sup> NSCL, Michigan State University, East Lansing, MI 48824, USA

<sup>h</sup> Department of Physics, Kyoto University, Kyoto 606-8502, Japan

<sup>i</sup> Argonne National Laboratory, Argonne, IL 60439, USA

<sup>j</sup> Department of Physics, Osaka University, Osaka 560-0043, Japan

<sup>k</sup> Department of Physics, Kyushu University, Fukuoka 812-8581, Japan

### ARTICLE INFO

#### Article history:

Received 18 October 2007

Received in revised form 27 June 2008

Accepted 15 July 2008

Available online 26 July 2008

Editor: D.F. Geesaman

#### PACS:

21.10.Pc

25.55.Hp

27.20.+n

29.30.Kv

#### Keywords:

Intruder state

Proton single particle state

Proton transfer reaction

$^4\text{He}(^{12}\text{Be}, ^{13}\text{B}\gamma)$

### ABSTRACT

The neutron-rich nucleus  $^{13}\text{B}$  was studied via the proton transfer reaction  $^4\text{He}(^{12}\text{Be}, ^{13}\text{B}\gamma)$  at 50 A MeV. The known 4.83-MeV excited state was strongly populated and its spin and parity were assigned to  $1/2^+$  by comparing the angular differential cross section data with DWBA calculations. This low-lying  $1/2^+$  state is interpreted as a proton intruder state and indicates a deformation of the nucleus.

© 2008 Elsevier B.V. All rights reserved.

The existence of intruder states in light neutron-rich unstable nuclei is often considered to be evidence for one or more  $\hbar\omega$  configurations in the low-lying states around the *psd* shell. The ground state of  $^{11}\text{Be}$  is  $1/2^+$  which is lower in energy by 0.3 MeV than the  $1/2^-$  state [1]. In  $^{12}\text{Be}$ , there is a  $1^-$  intruder state at 2.7-MeV excitation energy [2]. The energies of these low-lying, non-normal parity states indicate  $1\hbar\omega$  configurations. Furthermore, the presence of low-lying  $2_1^+$  [3] and  $0_2^+$  [4,5] states in  $^{12}\text{Be}$  suggests a  $2\hbar\omega$  configuration.

Three theoretical interpretations have been proposed for these one or more  $\hbar\omega$  configurations in the low-lying states of neutron-rich unstable nuclei: (1) the monopole interaction of the tensor force [6], (2) the loosely bound nature of some orbitals [7], and (3) nuclear deformation [5,8,9]. In Ref. [6], the effective interaction was determined so that the model reproduces the energy levels in light, neutron-rich nuclei including intruder states, and the importance of monopole interaction due to the tensor force was pointed out. Ref. [7] discusses the fact that in the *psd* shell, the  $2s_{1/2}$  orbital gains its energy relative to the other orbitals due to its loosely bound nature. The non-zero  $\hbar\omega$  configurations can also be intuitively explained by the deformed mean field picture. As seen in the Nilsson diagram, the gap becomes smaller with increasing deformation [5,8,9]. Since the combination of these effects, which

\* Corresponding author.

E-mail address: ota@cns.s.u-tokyo.ac.jp (S. Ota).

are provided by their corresponding theoretical models, changes the neutron shell structure in neutron-rich nuclei, such as  $^{11,12}\text{Be}$ , the relative importance of the three theoretical approaches has not been clarified.

For the proton shell in light neutron-rich nuclei, the effects due to the tensor force and the loosely bound nature of the orbitals are expected to be small since the  $\nu p_{1/2,3/2}$  orbitals are fully filled and the proton(s) are deeply bound. However, deformation is still presumed to affect the proton shell structure. Proton intruder states are, therefore, signatures for the importance of deformation. In the present Letter, we focus on the proton shell structure in the  $N = 8$  nucleus  $^{13}\text{B}$  by investigating the proton single-particle states.

In order to investigate the proton single-particle states in  $^{13}\text{B}$ , we used the  $(\alpha, t)$  reaction on  $^{12}\text{Be}$  in inverse kinematics. This process at an intermediate energy has a relatively large cross section since the proton to be transferred is deeply bound in the  $\alpha$  particle and, thus, has high-momentum components, which reduce the effect of the momentum mismatch of the  $(\alpha, t)$  reaction [10].

The experiment was performed at the RIKEN Accelerator Research Facility. A  $^{12}\text{Be}$  beam was produced by the fragmentation reaction of a 100 A MeV  $^{18}\text{O}$  beam on a  $^9\text{Be}$  target with a thickness of 1.85 g/cm $^2$ . The  $^{12}\text{Be}$  beam was separated by the RIKEN Projectile-fragment Separator (RIPS) [12]. The incident particles were identified on an event-by-event basis using the measured time-of-flight and the energy deposited. The time-of-flight, over a path length of 5.4 m, and the energy deposited were measured using two plastic scintillators located at the last two foci of the RIPS. The intensity and the purity of the  $^{12}\text{Be}$  beam respectively were typically  $2 \times 10^5$  counts per second and 90%.

The 50 A MeV  $^{12}\text{Be}$  beam bombarded a secondary target of liquid helium [11] located at the final focus of the RIPS. A liquid helium target was chosen because of its statistical advantage in terms of the experimental yields. The helium was condensed by a cryogenic refrigerator and kept below 4 K during the experiment. A target thickness of  $143 \pm 5$  mg/cm $^2$  was estimated from the velocity difference between outgoing particles measured with and without the liquid helium. The positions and directions of the incident particles on the secondary target were deduced from the position information of two parallel plate avalanche counters [13] located 30 cm apart from each other around the final focus. The outgoing particles were detected by a plastic scintillator hodoscope 3.5 m downstream from the secondary target with a  $1 \times 1$  m $^2$  active area and an angular acceptance of up to 8 degrees in the laboratory frame. The plastic scintillator hodoscope consisted of 5-mm thick  $\Delta E$  and 60-mm thick  $E$  layers. The  $\Delta E$  layer was divided into 13 plastic scintillator bars vertically and the  $E$  layer into 16 plastic scintillator bars horizontally. The outgoing particles were identified on an event-by-event basis using the measured time-of-flight and the energy deposited in the  $\Delta E$  and  $E$  layers. The mass distribution for the  $Z = 5$  particles is shown in Fig. 1; the mass resolution ( $\delta A$ ) was determined to be  $\sim 0.25$ . The time-of-flight between the secondary target and the hodoscope was deduced from the time information of the plastic scintillators located upstream from the secondary target and the plastic scintillator hodoscope. Position information for the outgoing particles was deduced from the time difference between the output signals from the two photomultiplier tubes attached to both ends of each scintillator bar, and was used to determine the scattering angle. The angular resolution of the scattering angle in the laboratory frame was 0.5 degrees in one standard deviation.

The de-excitation  $\gamma$  rays were detected by an array of germanium detectors: Gamma-Ray detector Array with Position and Energy sensitivities (GRAPE) [14]. This consisted of 6 germanium detectors located at  $140^\circ$  with respect to the beam axis. Each detector contains two cylindrical crystals 6 cm in diameter and 2 cm thick, with a common anode between them. The each cathode at-

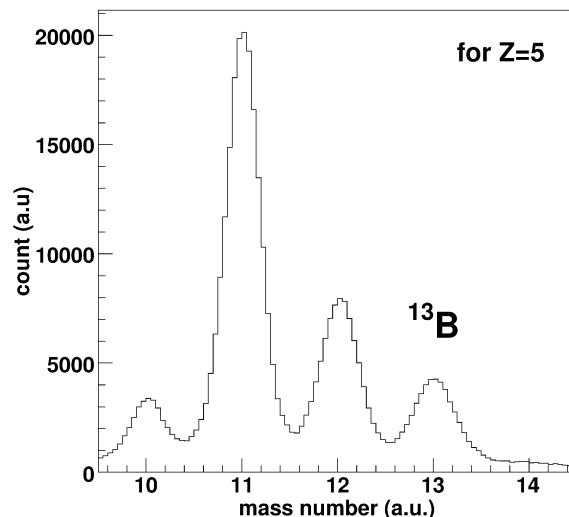


Fig. 1. Mass distribution of the outgoing particles for  $Z = 5$  extracted from the correlation between TOF and  $\Delta E$  measured with the plastic scintillator hodoscope.

tached to each crystal is segmented into a  $3 \times 3$  matrix. The GRAPE provides position information of the  $\gamma$ -ray interaction point, which is extracted from a pulse shape analysis of the signal from the cathode [14,15]. The intrinsic energy resolution and the full energy peak efficiency were typically 2.7 keV (FWHM) and 0.4%, respectively, for 1332-keV  $\gamma$  rays from a  $^{60}\text{Co}$  standard source. The energy resolution after correcting for the Doppler shift was deduced to be 1.3% (FWHM) for 2.1-MeV  $\gamma$  rays, corresponding to the decay of the first  $2^+$  state of  $^{12}\text{Be}$  moving with 30% the light velocity. The excited states of  $^{13}\text{B}$  populated in the reaction were identified by measuring the energy of the de-excitation  $\gamma$  rays.

Fig. 2 shows the energy spectrum of  $\gamma$  rays measured in coincidence with  $^{13}\text{B}$  after correcting for the Doppler shift. There are three peaks corresponding to the transitions from (3.68-, 3.73-), 4.13- and 4.83-MeV excited states to the ground state. The peaks seen in the low energy region are considered to originate from the reaction of the beam and the window of the target cell. Other significant transitions including those between the excited states were not observed in the present measurement. In the figure, hatched areas show the response functions of the GRAPE for the de-excitation  $\gamma$  rays obtained by means of a Monte Carlo simulation using the GEANT4 code [16,17] and for the background  $\gamma$  rays. The background was assumed to consist of two components, the natural background  $\gamma$  rays, estimated by putting the gate in the non-prompt region of the time spectrum of the GRAPE, and the  $\gamma$  rays from the isomer state of  $^{12}\text{Be}$ , which were simulated by assuming a life time of 331 ns [5]. The ratio of the isomer state to the ground state in the secondary beam was less than 2 percent at the secondary target. In the simulations, all the resolutions of the detectors associated with the correction for the Doppler shift were taken into account. The intensity of each decay to the ground state was deduced by fitting the experimental spectrum with the sum of the response functions and the background. Assuming no cascade decay, the derived relative intensities of the observed  $\gamma$  rays from the known excited states are shown in Table 1, together with the previously reported data including two neutron transfer [18], neutron knockout [19],  $\beta$ -decay followed by neutron decay [20], and multi-nucleon transfer [21]. In the present reaction, the excited state at 4.83 MeV is strongly populated relative to the other excited states, while it is less excited in the other reactions except for the multi-nucleon transfer reaction which is expected to populate proton excited states. Considering the selectivity of the proton

Download English Version:

<https://daneshyari.com/en/article/1852281>

Download Persian Version:

<https://daneshyari.com/article/1852281>

[Daneshyari.com](https://daneshyari.com)